Check for updates

Experimental Investigation and Theoretical Model for Subcooled Flow Boiling Pressure Drop in Microchannel Heat Sinks

Jaeseon Lee
United Technologies Research Center,
East Hartford, CT 06108
e-mail: leejs@utrc.utc.com

Issam Mudawar[1]
Boiling and Two-Phase Flow Laboratory (BTPFL),
Purdue University International Electronic
Cooling Alliance (PUIECA),
Mechanical Engineering Building,
585 Purdue Mall,
West Lafayette, IN 47907-2088
e-mail: mudawar@ecn.purdue.edu

This study examines the pressure drop characteristics of subcooled two-phase microchannel heat sinks. A new model is proposed, which depicts the subcooled flow as consisting of a homogeneous two-phase flow layer near the heated walls of the microchannel and a second subcooled bulk liquid layer. This model is intended for conditions where subcooled flow boiling persists along the entire microchannel and the outlet fluid never reaches bulk saturation temperature. Mass, momentum, and energy control volume conservation equations are combined to predict flow characteristics for thermodynamic equilibrium qualities below zero. By incorporating a relation for apparent quality across the two-phase layer and a new criterion for bubble departure, this model enables the determination of axial variations in two-phase layer thickness and velocity as well as pressure drop. The model predictions are compared with HFE 7100 pressure drop data for four different microchannel sizes with hydraulic diameters of 176–416 μm, mass velocities of 670–5550 kg/m² s, and inlet temperatures of 0°C and −30°C. The pressure drop database is predicted with a mean absolute error of 14.9%. [DOI: 10.1115/1.3144146]

1 Introduction

Today, there is an urgent need for innovative thermal management solutions that can tackle the high flux heat dissipation of high-end electronic and power devices. Heat removal rates from microprocessors surpassed 100 W/cm², while specialized devices in defense applications such as lasers, microwave systems, and radars are expected to exceed 1000 W/cm² [1]. Aside from dissipating the heat, device temperatures must be maintained below levels that are dictated by material and reliability concerns.

Most recent high flux cooling studies have been focused on phase-change schemes such as microchannel heat sinks and jet impingement. Yet, even with the high heat transfer coefficients achievable with these cooling schemes, very high flux heat dissipation renders the task of maintaining acceptable temperatures exceedingly difficult. An effective solution to this problem is to greatly lower the temperature of the coolant using direct or indirect refrigeration cooling. Vapor compression systems are ideally suited for this purpose as they provide adequate cooling capacity at temperatures as low as −100°C. Recently, the authors of the present study examined the performance of a direct refrigeration cooling system in which the electronic device was cooled by refrigerant flowing through a miniature microchannel evaporator [2–4].

The dominant heat transfer mechanism in microchannel flows remains quite illusive. Recent studies in this area point to one of two fundamentally different mechanisms. Commonly cited in the vast majority of recent articles, the first mechanism is described as annular film evaporation evidenced by decreasing value of the convective heat transfer coefficient with increasing quality as well as dependence on mass velocity [5–12]. The second mechanism is described as dominated by nucleate boiling evidenced by the dependence of the heat transfer coefficient on heat flux but not mass velocity or quality [13–18]. As discussed in this study, the discrepancy between the two mechanisms may be explained by different coolants, operating conditions, and/or channel sizes used by different investigators yielding different dominant mechanisms.

The present study examines an indirect refrigeration cooling system, where the primary coolant flowing through the microchannel heat sink rejects its heat via a heat exchanger to refrigerant of a separate vapor compression loop. With a high degree of subcooling, flow boiling behavior of the primary coolant inside the microchannel heat sink is categorically different from the annular flow mechanism discussed in the vast majority of articles written about two-phase microchannel heat sinks. Those earlier studies involve high void fractions and saturated flow boiling. The present study concerns highly subcooled flow boiling, where subzero quality is preserved even as the fluid exits the microchannels. Here, vapor is formed by nucleation at the wall with a highly subcooled liquid core flow. Severe departure from thermodynamic equilibrium renders modeling of two-phase flow in this case highly elusive.

Pressure drop is a key parameter in the design of a two-phase cooling system. Pressure drop in subcooled flow boiling consists of frictional and accelerational components and the magnitude of each is highly dependent on void fraction. Departure from thermodynamic equilibrium greatly complicates the task of relating void fraction to flow quality, which is the primary reason behind the difficulty predicting pressure drop in subcooled flow boiling.

Nonequilibrium effects in subcooled flow boiling, especially the prediction of void fraction, is a very complex topic that was historically tackled only in a handful of macrochannel publications dating back to the 1960s and 1970s, e.g., Refs. [19–22]. A recent study by Hoffman and Wong [23] showed these models yield poor predictions of pressure drop.

The present study is the first attempt at developing a theoretical control-volume-based model for subcooled flow boiling pressure drop. Control-volume-based models were quite effective at predicting both pressure drop and heat transfer in saturated flow boiling in microchannel heat sinks [24,25] as well as flow boiling critical heat flux [26]. The model proposed in this study is particularly suited for situations involving severe nonequilibrium between the vapor and liquid phases.

[1]Corresponding author.

Contributed by the Electrical and Electronic Packaging Division of ASME for publication in the JOURNAL OF ELECTRONIC PACKAGING. Manuscript received December 17, 2007; final manuscript received March 5, 2009; published online July 2, 2009. Assoc. Editor: Xiaoling He.

 Copyright © 2009 by ASME

Downloaded from https://asmedigitalcollection.asme.org/electronicpackaging/article-pdf/131/3/031008/5656138/031008_1.pdf by Purdue University at West Lafayette user on 22 October 2019

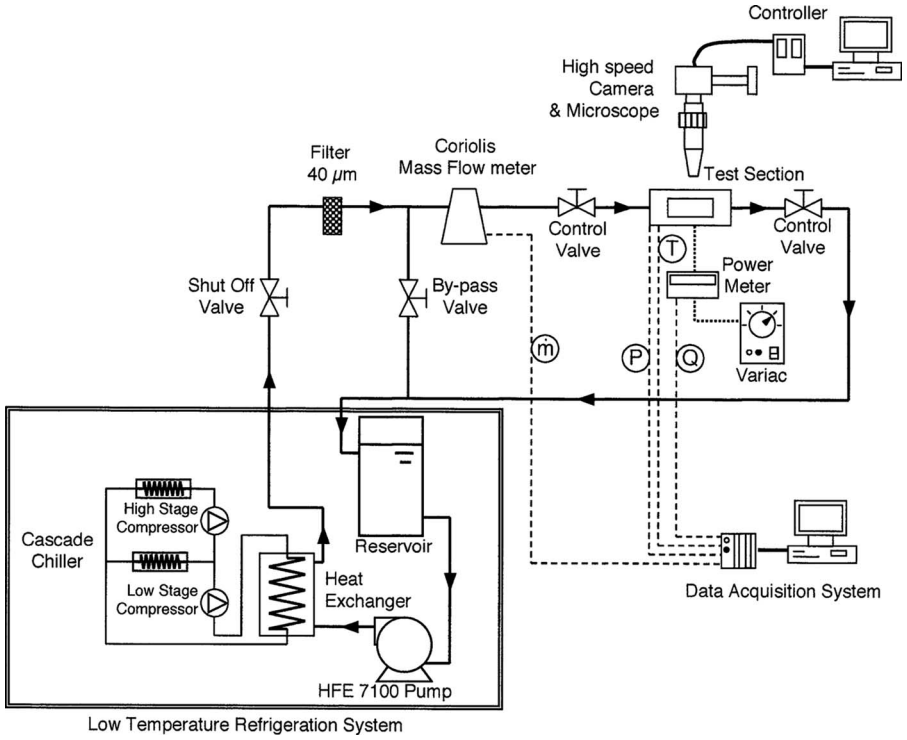

Fig. 1 Flow diagram for indirect refrigeration cooling system

2 Experimental Methods

2.1 Flow Loop and Test Section. Figure 1 shows a schematic of the two-phase facility developed for this study. The facility consisted of two main subsystems, a primary loop in which the microchannel test section (TS) was inserted and a refrigeration loop that was used to reduce the temperature of the working fluid, HFE 7100, in the primary loop. This 3M Novec fluid has very low freezing point (below −100°C) and a relatively moderate boiling point of 60°C at atmospheric pressure. It has excellent dielectric properties, zero ozone depletion potential, and unusually low global warming potential, which is very inert, and its surface tension is much smaller than that of water. Table 1 provides key thermal properties of HFE 7100.

As shown in Fig. 1, HFE 7100 is circulated through the primary loop with the aid of a centrifugal pump. This primary coolant is pumped from a reservoir through a heat exchanger where its temperature is reduced by heat transfer to the secondary refrigeration loop. The HFE 7100 then passes through a filter followed by a Coriolis mass flow meter before entering the microchannel test section. Throttling valves situated both upstream and downstream of the test section are used to control both flow rate and exit pressure. The HFE 7100 then returns to the reservoir, completing a full cycle.

Table 1 Summary of thermophysical properties of HFE 7100

	k_f (W/m K)	μ_f (kg/m s)	$c_{p,f}$ (J/kg K)	σ (mN/m)
$T=-30°C$	0.0796	14.74×10^{-4}	1073.0	18.2
$T=0°C$	0.0737	8.26×10^{-4}	1133.0	15.7

	T_{sat} (°C)	h_f (kJ/kg)	h_{fg} (kJ/kg)	ρ_f (kg/m^3)	ρ_g (kg/m^3)
$P=1.0$ bar	59.63	92.76	111.7	1372.7	9.58
$P=3.5$ bars	104.41	145.5	97.61	1238.9	32.14

Figure 2 depicts the construction of the microchannel test section. Microchannels with rectangular cross section are cut into the top surface of an oxygen-free copper block with the aid of thin carbide blades. The large lower section of the copper block is bored to accommodate four high-power-density cartridge heaters. The smaller top portion of the copper block is inserted into a rectangular housing made from G-11 fiberglass plastic that features coolant inlet and outlet ports, microchannel inlet and outlet plenums, and both pressure and temperature instrumentation ports. The microchannels are formed after the grooves in the top surface of the copper block are sealed with a transparent plastic cover plate. All outer surfaces of the copper block are carefully insulated to minimize heat loss to the ambient.

To examine the effects of microchannel geometry on pressure drop, four different copper blocks were machined, each having different microchannel dimensions. All four copper blocks have the same top 0.5 cm wide by 1.0 cm long heat transfer area. Table 2 provides detailed dimensions of the four test sections.

2.2 Operating Conditions and Measurements. The temperature of HFE 7100 at the heat exchanger outlet in the primary loop is accurately maintained to within ±0.5°C by automatic feedback control of the secondary loop vapor compression chiller. Tests were performed with a constant test module outlet pressure of 1.138 bars and two different inlet temperatures, −30°C and 0°C. Lower temperatures were possible but avoided because of frost formation on the test section's transparent cover plate below −30°C. The experiments were conducted at different flow rates. For each test, heat flux was increased gradually to generate a boiling curve, which, for some tests, continued to the critical heat flux (CHF) point. Table 3 provided ranges of all parameters of the study.

The test section's instrumentation included pressure transducers and thermocouples for both the inlet and outlet plenums. Three type-T thermocouples were inserted in the copper block beneath

Downloaded from https://asmedigitalcollection.asme.org/electronicpackaging/article-pdf/131/3/031008/5656138/031008_1.pdf by Purdue University at West Lafayette user on 22 October 2019

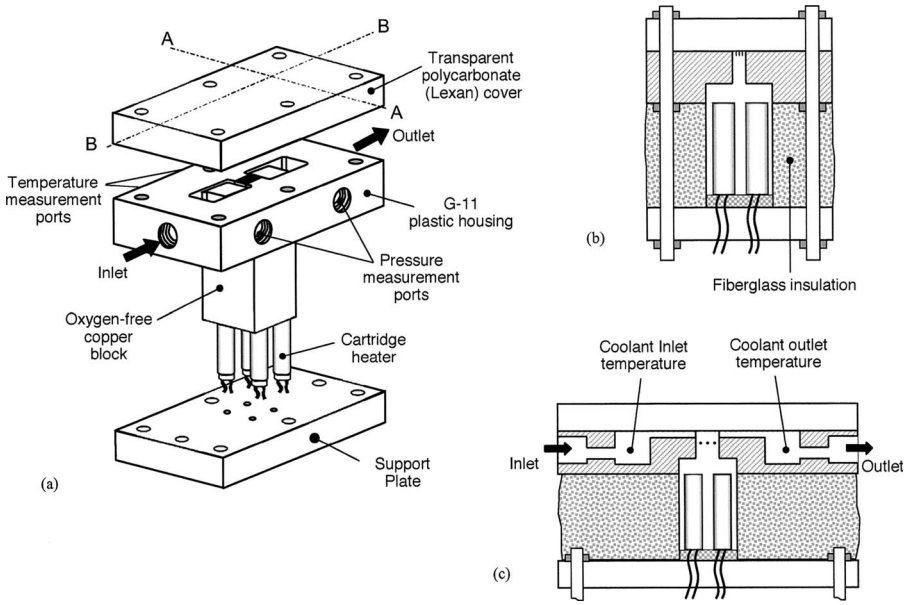

Fig. 2 (*a*) Isometric view of microchannel test section, (*b*) cross-sectional view (A-A), and (*c*) side sectional view (B-B)

the microchannels. Other measurements included electrical power input to the test section's four cartridge heaters using a wattmeter and mass flow rate using a Coriolis flow meter. All measurements were made simultaneously and processed by an HP3852 data acquisition system.

Because of heat loss, not all the measured electrical power input to the cartridge heater was transferred to the coolant flowing through the test section. To estimate the heat loss, a finite element model of the entire test section and surrounding insulation was constructed in which local convective heat transfer coefficients were first determined from the measured electrical power input and copper block temperatures. Heat loss was then calculated from the model and heat transfer coefficient values were updated after deducting heat loss from the power input. Several iterations were used until the solution converged. Heat loss was estimated at 14–20% of the electrical power input for single-phase conditions and 6–14% for double-phase conditions. The heat flux data presented in this study were all corrected for this heat loss. Additional details concerning the heat loss calculation are available in a previous paper by the authors [27].

Uncertainties in the temperature measurements were $\pm 0.5^\circ$C for inlet fluid temperature control and $\pm 0.3^\circ$C for thermocouple readings. Accuracies of other measurement instruments were as follows: $\pm 0.5\%$ for the pressure transducers, $\pm 0.1\%$ for the Coriolis flow meter, and $\pm 0.1\%$ for the wattmeter.

Table 2 Test section dimensions

	W_{ch} (μm)	W_w (μm)	H_{ch} (μm)	AR	D_h (μm)	L (cm)	N
TS No. 1	123.4	84.2	304.9	2.47	175.7	1.0	24
TS No. 2	123.4	84.6	526.9	4.27	200.0	1.0	24
TS No. 3	235.2	230.3	576.8	2.45	334.1	1.0	11
TS No. 4	259.9	205.0	1041.3	4.01	415.9	1.0	11

Table 3 Experimental operating conditions

	T_{in} (°C)	$\dot{m}$ (g/s)	P_{out} (bar)	G (kg/m^2 s)	Re_{Dh}	q'' (W/cm^2)
TS No. 1	−30, 0	2.0–5.0	1.138	2200–5550	265–1170	0–560
TS No. 2	−30, 0	2.0–5.0	1.138	1280–3210	175–780	0–580
TS No. 3	−30, 0	2.0–5.0	1.138	1330–3350	304–1360	0–640
TS No. 4	−30, 0	2.0–20.0	1.138	670–6730	189–3370	0–750

3 Developing Homogeneous Layer Model

3.1 Model Description and Assumptions. Subcooled flow boiling is initiated when bubbles begin to nucleate in a mostly subcooled liquid flow and extends to the axial location where thermodynamic equilibrium quality reaches zero. The subcooled flow boiling region consists of two subregions, a highly subcooled subregion and a developing subcooled subregion. Vapor void in the highly subcooled subregion is a wall effect since strong condensation effects along the bubble interface suppress bubble growth and prevent coalescence between bubbles. The developing subcooled subregion is initiated at the point of bubble detachment off the heating wall. Here, bubbles are able to grow and depart into the subcooled liquid stream.

Prior studies by the other authors shed some light on the unique nature of subcooled boiling in microchannels [27]. Unlike flow in long macrochannels, the transition from single-phase liquid flow or highly subcooled flow to developing subcooled boiling in short microchannels results occurs abruptly after a relatively mild increase in heat flux. Furthermore, because of both small channel size and heat flux controlled boundary condition, the subcooled boiling region engulfs the entire length of the microchannel at once. The authors' past flow visualization studies show that subcooled flow boiling inside the microchannels is dominated by bubbly flow and, to a lesser extent, slug flow. These studies also showed that vapor flow is initiated by bubbles that nucleate upstream, remaining close to the wall. The vapor void fraction increases gradually, culminating in bubbly flow that traverses the entire microchannel cross section downstream. This vapor development pattern constitutes the main rationale for the present model.

Figure 3 shows a schematic representation of the *developing homogeneous layer model* (DHLM) adopted in this study. This model is constructed specifically for developing subcooled flow boiling in microchannels and should be extended to neither the single-phase region nor the saturated boiling region. This model considers conditions where developed subcooled boiling engulfs

Downloaded from https://asmedigitalcollection.asme.org/electronicpackaging/article-pdf/131/3/031008/5656138/031008_1.pdf by Purdue University at West Lafayette user on 22 October 2019

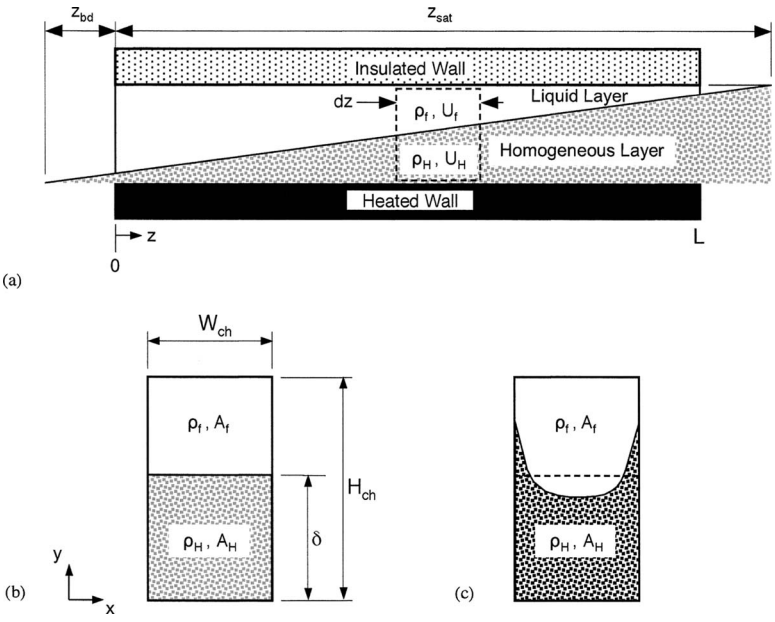

Fig. 3 (*a*) Side view and (*b*) cross-sectional view representation of DHLM. (*c*) Cross-sectional view of the actual interface between homogeneous two-phase layer and liquid layer in the presence of sidewall heating effects.

the entire length of the microchannels. Thus, it precludes an upstream single-phase region or downstream saturated boiling region along the heated wall. Extension of the developing subcooled boiling layer both upstream and downstream of the heated length as shown in Fig. 3(*a*) will be discussed later.

DHLM assumes that flow consists of two layers, a subcooled liquid core and a homogeneous two-phase flow layer; the latter represents the bubbly region of the flow. The homogeneous layer thickens along the flow direction due to wall heating. Key assumptions of the model are as follows.

(1) The flow is one-dimensional, meaning flow velocity in each layer is constant at any axial location.
(2) The flow is steady.
(3) The liquid layer flow is laminar and incompressible. Also, because of the large density and relatively strong momentum of liquid relative to the two-phase layer, as well as the relatively short length of the microchannel, the liquid velocity is assumed constant along the flow direction.
(4) The two-phase layer behaves as a homogeneous two-phase mixture whose properties are weighted averages of those of liquid and vapor.
(5) There is no thermal equilibrium between the two layers. The two-phase layer is assumed to maintain saturated temperature, while the liquid layer is subcooled. In the flow direction, heat supplied from the wall increases vapor quality in the homogenous layer and liquid temperature. Heat is also transferred between the two layers.
(6) Pressure is uniform across the flow area of the microchannel at every axial location.
(7) As shown in Fig. 3(*b*), an idealized flat interface is assumed between the homogeneous two-phase layer and the liquid layer to determine mean thickness of the two-phase layer from the model. As shown in Fig. 3(*c*), the actual interface is distorted by greater void toward the sidewalls and lesser void near the center of the microchannel because of heating from the sidewalls.

3.2 Control Volume Conservation Equations. Figure 4(*a*) shows mass flow terms for a microchannel control volume of length Δz along the flow direction. Mass conservations for the liquid layer and the homogeneous layer can be expressed, respectively, as

$$\frac{d(\rho_f U_f A_f)}{dz} + K_i = 0 \tag{1}$$

and

$$\frac{d(G_H A_H)}{dz} - K_i = 0 \tag{2}$$

where $G_H = \rho_H U_H$, the mass velocity of the homogeneous layer, and K_i is the rate of mass transfer from the liquid layer to the homogeneous layer per unit axial distance. Since liquid density is assumed constant, it can be taken out of the derivative in Eq. (1).

Figure 4(*b*) shows energy conservation for the homogeneous layer alone. Heat supplied from the wall is consumed in two different ways. A portion of this heat increases the temperature of the liquid mass transferred between the liquid layer and the homogeneous layers from T_f to T_{sat}. The remaining portion increases the latent heat of the homogeneous layer. Therefore, energy conservation for the homogenous layer can be expressed as

$$q''(W_{ch} + W_w) = \frac{d}{dz}(G_H A_H h_H) + K_i c_{p,f}(T_{sat} - T_f) \tag{3}$$

Because of the subcooled boiling state of the flow, the enthalpy h_H of the homogeneous layer requires careful assessment. This issue will be discussed in Sec. 3.3.

Figure 5 shows the momentum changes and forces acting on the control volume. Momentum conservation for the liquid layer and the homogeneous layer can be expressed, respectively, as

$$\frac{d(\rho_f U_f^2 A_f)}{dz} + K_i U_i = -A_f \frac{dP}{dz} - P\frac{dA_f}{dz} - \tau_{f,w}[W_{ch} + 2(H_{ch} - \delta)] - \tau_i W_{ch} \tag{4}$$

and

Downloaded from https://asmedigitalcollection.asme.org/electronicpackaging/article-pdf/131/3/031008/5656138/031008_1.pdf by Purdue University at West Lafayette user on 22 October 2019

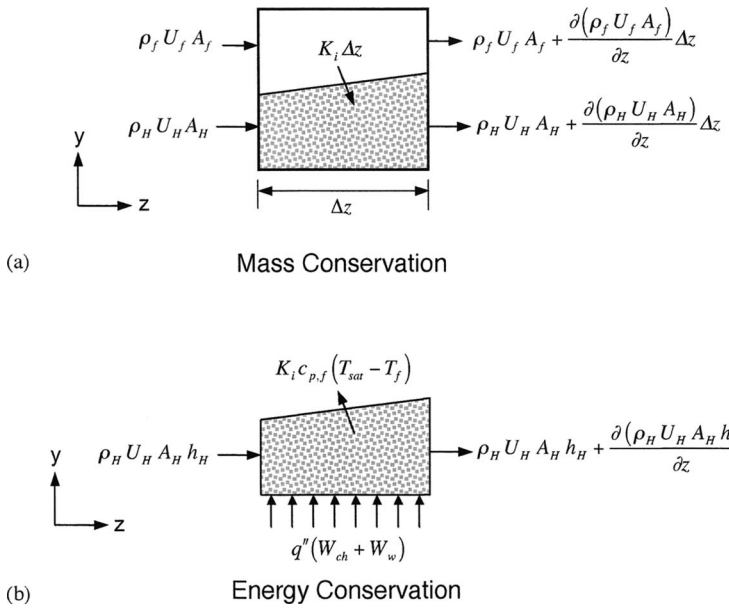

Fig. 4 (*a*) Mass conservation for liquid and homogeneous layer control volumes and (*b*) energy conservation for homogenous layer control volume

$$\frac{d(\rho_H U_H^2 A_H)}{dz} - K_i U_i = -A_H \frac{dP}{dz} - P\frac{dA_H}{dz} - \tau_{H,w}[W_{\text{ch}} + 2\delta] + \tau_i W_{\text{ch}} \tag{5}$$

Combining Eqs. (4) and (5) eliminates both the interfacial momentum and interfacial friction terms, resulting in the following equation:

$$\frac{d(\rho_f U_f^2 A_f)}{dz} + \frac{d(\rho_H U_H^2 A_H)}{dz} = -A\frac{dP}{dz} - \{\tau_{f,w}[W_{\text{ch}} + 2(H_{\text{ch}} - \delta)] + \tau_{H,w}[W_{\text{ch}} + 2\delta]\} \tag{6}$$

Equations (1)–(3) and (6) are the main governing equations for DHLM.

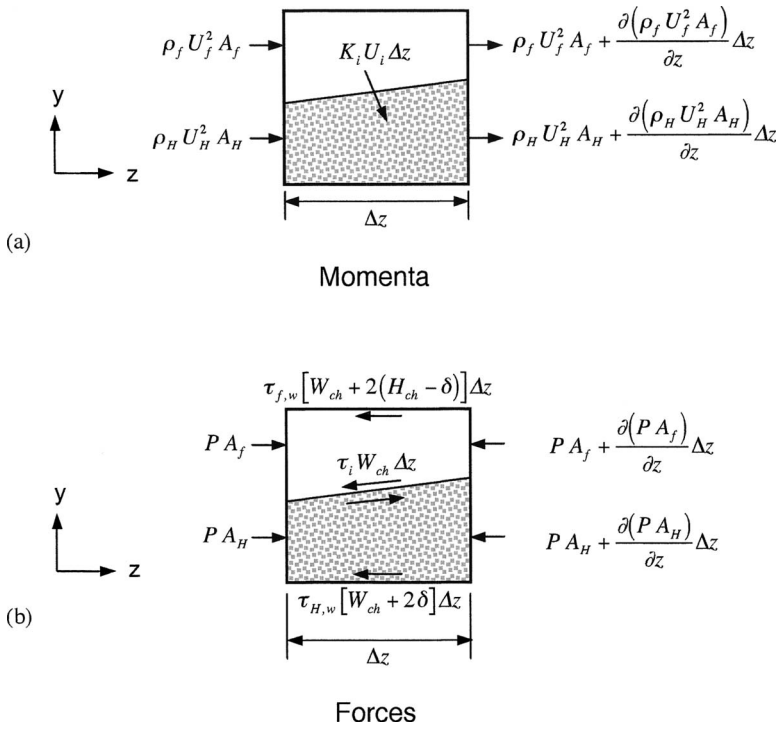

Fig. 5 (*a*) Moments and (*b*) forces for liquid and homogeneous layer control volumes

Downloaded from https://asmedigitalcollection.asme.org/electronicpackaging/article-pdf/131/3/031008/5656138/031008_1.pdf by Purdue University at West Lafayette user on 22 October 2019

Table 4 Additional relations of DHLM

	Equations	
Two-phase density	$\rho_H = \dfrac{1}{\dfrac{x'}{\rho_g} + \dfrac{1-x'}{\rho_f}}$	(25)
Two-phase viscosity (McAdams model)	$\mu_H = \dfrac{1}{\dfrac{x'}{\mu_g} + \dfrac{1-x'}{\mu_f}}$	(26)
	$\tau_{f,w} = \dfrac{1}{2} f_f \rho_f U_f^2$	(27)
	$f_f \operatorname{Re}_f = \left\{ 3.44 z_{hy}^{+-0.5} + \dfrac{1.089/4 z_{hy}^{+} + K_f - 3.44/z_{hy}^{+0.5}}{1 + 0.000131 z_{hy}^{+-2}} \right\}$	(28)
Liquid layer wall shear [28]	$\operatorname{Re}_f = \dfrac{\rho_f U_f D_{h,f}}{\mu_f}$	(29)
	$D_{h,f} = \dfrac{2(H_{\mathrm{ch}} - \delta) W_{\mathrm{ch}}}{(H_{\mathrm{ch}} - \delta) + W_{\mathrm{ch}}}$	(30)
	$z_{hy}^{+} = \dfrac{z}{D_h \operatorname{Re}_f}$	(31)
	$K_f = 24(1 - 1.355\beta_f + 1.947\beta_f^2 - 1.701\beta_f^3 + 0.956\beta_f^4 - 0.254\beta_f^5)$	(32)
	$\beta_f = \dfrac{W_{\mathrm{ch}}}{(H_{\mathrm{ch}} - \delta)} \quad \text{or} \quad \dfrac{(H_{\mathrm{ch}} - \delta)}{W_{\mathrm{ch}}}, \quad \beta_f \le 1$	(33)
	$\tau_{H,w} = \dfrac{1}{2} f_H \rho_H U_H^2$	(34)
	$f_H = \dfrac{K_H}{\operatorname{Re}_H}$	(35)
Homogeneous layer wall shear	$\operatorname{Re}_H = \dfrac{\rho_H U_H D_{h,H}}{\mu_H}$	(36)
	$D_{h,H} = \dfrac{2\delta W_{\mathrm{ch}}}{\delta + W_{\mathrm{ch}}}$	(37)
	$K_H = 24(1 - 1.355\beta_H + 1.947\beta_H^2 - 1.701\beta_H^3 + 0.956\beta_H^4 - 0.254\beta_H^5)$	(38)
	$\beta_H = \dfrac{W_{\mathrm{ch}}}{\delta} \quad \text{or} \quad \dfrac{\delta}{W_{\mathrm{ch}}}, \quad \beta_H \le 1$	(39)

3.3 Solution Scheme. Referring to Fig. 3(*b*) the flow areas for the liquid layer and the homogeneous layer can be expressed, respectively, as

$$A_f = W_{\mathrm{ch}}(H_{\mathrm{ch}} - \delta) \tag{7}$$

and

$$A_H = W_{\mathrm{ch}}\delta \tag{8}$$

Therefore, the area derivatives with respect to z can be expressed as

$$\frac{dA_f}{dz} = -W_{\mathrm{ch}}\frac{d\delta}{dz} \tag{9}$$

and

$$\frac{dA_H}{dz} = W_{\mathrm{ch}}\frac{d\delta}{dz} \tag{10}$$

Based on the assumptions of DHLM, the liquid layer preserves its velocity along the microchannel. Therefore,

$$U_f = \frac{G}{\rho_f} \tag{11}$$

and

$$\frac{dU_f}{dz} = 0 \tag{12}$$

where G is the mass velocity of the incoming subcooled nonboiling liquid. Since both ρ_f and U_f are constant along the flow direction, Eq. (1) yields

$$K_i = -\rho_f U_f \frac{dA_f}{dz} \tag{13}$$

Introducing the above relation in Eq. (9) gives

$$K_i = \rho_f U_f W_{\mathrm{ch}}\frac{d\delta}{dz} \tag{14}$$

Combining Eq. (14) with Eqs. (2), (8), and (10) gives

$$\frac{d\delta}{dz} = \frac{\delta\dfrac{dG_H}{dz}}{(\rho_f U_f - G_H)} \tag{15}$$

One of the key parameters in DHLM is the enthalpy h_H of the homogeneous two-phase layer. Because vapor is generated along the microchannel in a subcooled boiling region, thermodynamic equilibrium quality cannot be used to determine the enthalpy of the two-phase layer. Therefore, the enthalpy of this layer is defined as

$$h_H = h_f + x'_H h_{fg} \tag{16}$$

where x'_H is an *apparent* flow quality. Two different formulations

Downloaded from https://asmedigitalcollection.asme.org/electronicpackaging/article-pdf/131/3/031008/5656138/031008_1.pdf by Purdue University at West Lafayette user on 22 October 2019

were recommended for apparent quality in subcooled boiling. Levy's [20] formulation was attempted but produced unrealistic predictions for microchannel flow. A second formulation by Kroeger and Zuber [22] was used here.

$$x'_H(z) = \frac{c_{p,f}\Delta T_{\text{sub,in}}(Z^+ - T^*)}{h_{fg} + c_{p,f}\Delta T_{\text{sub,in}}(1 - T^*)} \tag{17}$$

where

$$Z^+ = \frac{z + z_{\text{bd}}}{z_{\text{sat}} + z_{\text{bd}}} \tag{18}$$

and

$$T^* = \tanh(Z^+) \tag{19}$$

Now, two-phase flow apparent quality can be predetermined over the entire test section domain without calculation of other governing equation variables. Quality gradient is also required later but it can be easily obtained since quality values are set by Eq. (17).

Combining Eqs. (10) and (14)–(17) with energy conservation equation (3) yields

$$\frac{dG_H}{dz} = \frac{(\rho_f U_f - G_H)\left\{q''(W_{\text{ch}} + W_w) - W_{\text{ch}}\delta G_H h_{fg}\dfrac{dx'_H}{dz}\right\}}{GW_{\text{ch}}\delta[h_H + c_{p,f}(T_{\text{sat}} - T_f)]} \tag{20}$$

Another equation for homogeneous layer thickness δ can be determined by substituting Eq. (20) into Eq. (15).

$$\frac{d\delta}{dz} = \frac{q''(W_{\text{ch}} + W_w) - W_{\text{ch}}\delta G_H h_{fg}\dfrac{dx'_H}{dz}}{GW_{\text{ch}}[h_H + c_{p,f}(T_{\text{sat}} - T_f)]} \tag{21}$$

Equations (20) and (21) are coupled ordinary differential equations. Referring to Fig. 2(*a*), these equations must satisfy the following conditions:

$$\delta = \begin{cases} 0 & \text{at } z = -z_{\text{bd}} \\ H_{\text{ch}} & \text{at } z = z_{\text{sat}} \end{cases} \tag{22}$$

and

$$G_H = \begin{cases} 0 & \text{at } z = -z_{\text{bd}} \\ G & \text{at } z = z_{\text{sat}} \end{cases} \tag{23}$$

To meet those boundary conditions, the homogeneous two-phase layer is assumed to evolve from zero thickness at an *equivalent* distance $-z_{\text{bd}}$ associated with preheating the flow at the same heat flux supplied at the microchannel. The homogeneous layer is also assumed to engulf the entire cross section at another equivalent distance z_{sat} extending beyond the microchannel exit and where the flow is subjected to the same heat flux supplied at the microchannel.

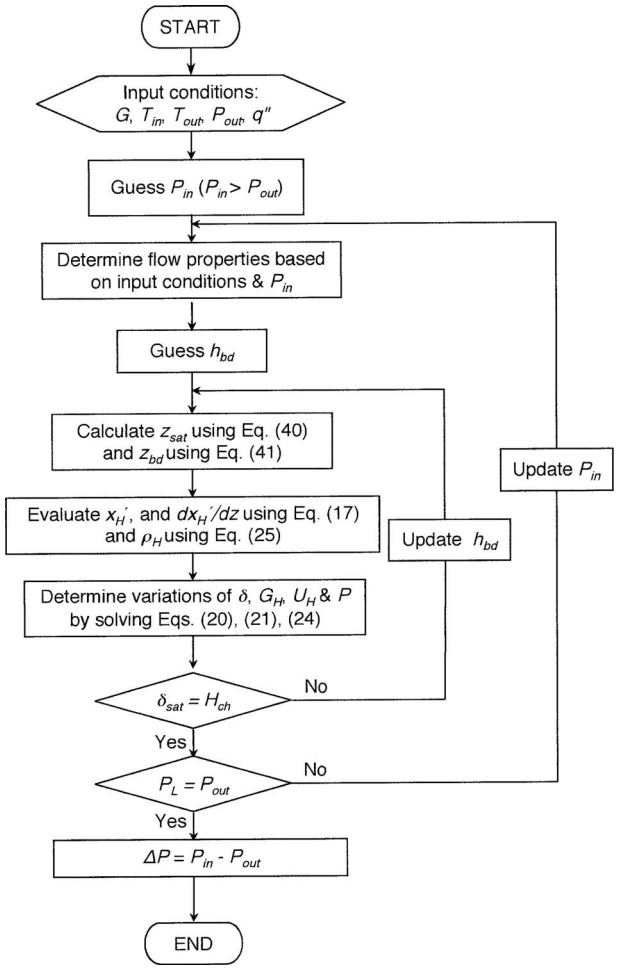

Fig. 6 Solution procedure for DHLM

Finally, Eqs. (9) and (10) are used along with $U_H = G_H/\rho_H$ to simplify the momentum equation (6) to the following explicit form:

$$\frac{dP}{dz} = -\frac{1}{W_{\text{ch}}H_{\text{ch}}}\left[-\rho_f U_f^2 W_{\text{ch}}\frac{d\delta}{dz} + \rho_H U_H^2 W_{\text{ch}}\frac{d\delta}{dz} + 2\rho_H U_H W_{\text{ch}}\delta\frac{dU_H}{dz} + U_H^2 W_{\text{ch}}\delta\frac{d\rho_H}{dz} + \{\tau_{f,w}[W_{\text{ch}} + 2(H_{\text{ch}} - \delta)] + \tau_{H,w}[W_{\text{ch}} + 2\delta]\}\right] \tag{24}$$

Notice that the solutions of Eqs. (20) and (21) are not dependent on Eq. (24). Therefore Eqs. (20) and (21) can be solved first for δ and G_H. Then the variations in δ, U_H, $d\delta/dz$, and dU_H/dz with z are substituted into Eq. (24) to solve separately for pressure drop. Two-phase density and its derivative are predetermined from the apparent quality calculations.

Several additional parameters are required to solve Eqs. (20), (21), and (24). They include mixture density and mixture viscosity of the homogeneous two-phase layer and friction factor relations for the liquid layer and the homogeneous layer specific to rectangular microchannels. These relations are summarized in Table 4. A more comprehensive discussion of homogeneous flow viscosity models is provided in a previous study by the authors [2].

There are also other parameters that define the domain of the subcooled boiling region. These parameters must be determined in advance. Referring to Fig. 3(*a*), the location of saturated boiling,

Downloaded from https://asmedigitalcollection.asme.org/electronicpackaging/article-pdf/131/3/031008/5656138/031008_1.pdf by Purdue University at West Lafayette user on 22 October 2019

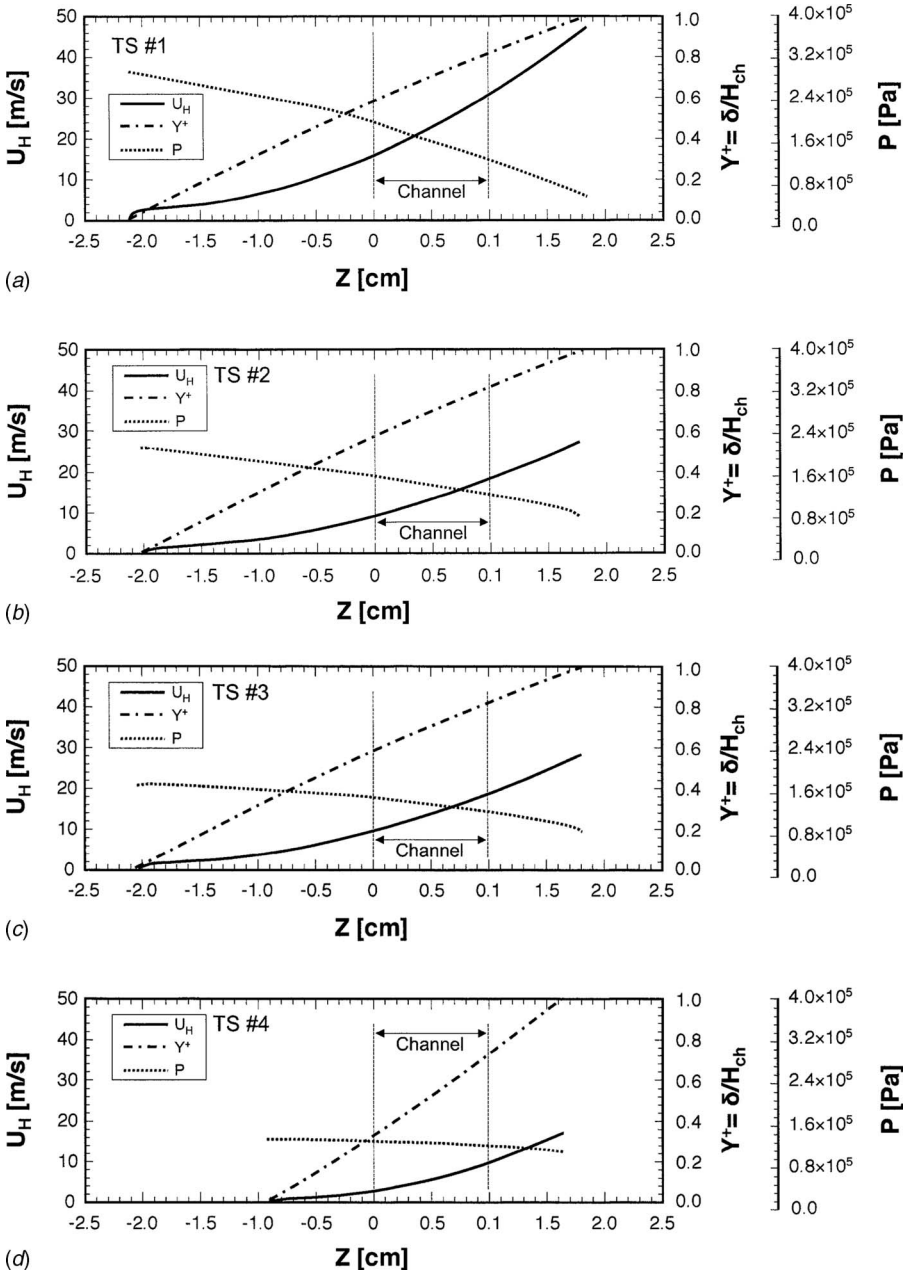

Fig. 7 DHLM predictions for $T_{in}=-30°C$ and $\dot{m}=5$ g/s for (*a*) TS No. 1 ($D_h=176$ μm) at $q''=561$ W/cm^2, (*b*) TS No. 2 ($D_h=200$ μm) at $q''=586$ W/cm^2, (*c*) TS No. 3 ($D_h=334$ μm) at $q''=560$ W/cm^2, and (*d*) TS No. 4 ($D_h=416$ μm) at $q''=627$ W/cm^2

which is also the downstream edge of DHLM domain, can be determined with the aid of a simple heat balance.

$$z_{sat}=\frac{GW_{ch}H_{ch}c_{p,f}(T_{sat}-T_{in})}{q''(W_{ch}+W_w)} \tag{40}$$

A key difficulty lies in the determination of z_{bd}. Two approaches are available from the literature for estimating the location of bubble departure. Both involve estimating flow subcooling $\Delta T_{sub,bd}$ at the departure point from which z_{bd} is calculated from the simple energy balance.

$$-z_{bd}=z_{sat}-\frac{\Delta T_{sub,bd}}{q''}\frac{GW_{ch}H_{ch}c_{p,f}}{(W_{ch}+W_w)} \tag{41}$$

Relations recommended by Bowring (Collier and Thome [29]) and Saha and Zuber [21] for $\Delta T_{sub,bd}$ for macrochannels produced poor predictions for the conditions of the present study. The bubble departure point was predicted with both relations to occur in the microchannel at much higher heat fluxes than actually measured.

An alternative relation for $\Delta T_{sub,bd}$ is suggested here that follows the same general form as the Saha and Zuber model but ensures the occurrence of bubble departure within the microchannel as captured experimentally in the authors' prior flow visualization studies [27].

$$\Delta T_{sub,bd}=\frac{q''C_G}{h_{bd}} \tag{42}$$

where h_{bd} is the heat transfer coefficient measured when bubble departure was first observed *inside* the microchannel, and C_G is a dimensionless function developed specifically for rectangular mi-

Downloaded from https://asmedigitalcollection.asme.org/electronicpackaging/article-pdf/131/3/031008/5656138/031008_1.pdf by Purdue University at West Lafayette user on 22 October 2019

crochannels and correlated with aspect ratio (AR) β from data for the four different test sections used in the present study.

$$C_G = 0.632\beta + 0.014 \tag{43}$$

The key challenge in using Eqs. (27) and (28)f is that the value of h_{bd} used to develop these correlations was measured experimentally for a condition that produced bubble departure inside the microchannel. However, as illustrated in Fig. 3(*a*), the value of h_{bd} sought in the DHLM is that of a pseudoheat transfer coefficient that yields bubble departure upstream of the microchannel. This value was determined with an iterative procedure described next.

Figure 6 outlines the entire solution procedure for DHLM. The model is initiated by guessing microchannel inlet pressure P_{in} at $z=0$, then h_{bd}. Different values of h_{bd} produced different variations in δ with z. The value of h_{bd} was updated until the model yielded $\delta=H$ at $z=z_{sat}$. Then the model used this last value of h_{bd} to determine the variation in P with z. Since the present experiments were performed with a fixed outlet plenum pressure ($P_{out}=1.138$ bars), the predicted microchannel exit pressure P_L at $z=L$ was corrected for pressure recovery due to expansion from the microchannels to the outlet plenum in order to determine P_{out}. If this value of P_{out} matched the measured pressure, the solution was deemed convergent. If, on the other hand, the pressure values did not agree, a new value of P_{in} was entered and the entire iteration repeated. Overall, pressure differences due to recovery were quite small and had virtually no impact on the pressure drop calculation. Details concerning two-phase pressure recovery relations are available in a paper by Qu and Mudawar [24].

4 Model Results

4.1 Profiles of Main Variables. Figure 7 shows predictions of the axial variations in the DHLM main variables: velocity of homogenous two-phase layer U_H, thickness of homogeneous layer δ, and pressure P for each of the four test sections. Notice that the profiles include the pseudo-upstream and downstream extensions of the subcooled boiling layer; the extent of the actual microchannel is indicated for each case. The results are based on the experimentally measured heat flux, which varies slightly between the four cases. Because of the relatively high heat flux, these conditions correspond to the upper range of the nucleate boiling region, which is indicated by the microchannel length corresponding to the relatively high void fraction region of the model domain.

Pressure drop across the microchannel is the difference between P_{in} predicted by DHLM at $z=0$ minus the measured outlet pressure P_{out} corrected for pressure recovery. Equation (24) shows that pressure drop is inversely proportional to the microchannel cross-sectional area and is strongly influenced by U_H. Figure 7 shows decreasing hydraulic diameter, which yields a substantial increase in U_H, increases pressure drop.

4.2 Validation of Model Predictions. Figure 8 compares pressure drop predictions of DHLM with measured pressure drop for the four test sections, two different flow rates, and two inlet temperatures. Most cases are predicted quite accurately with the exception of the largest hydraulic diameter at the higher inlet temperature. This shows the model is well suited to small rectangular microchannels and may begin to lose accuracy with large microchannels. The model's accuracy is apparently compromised when the homogenous two-phase layer assumption begins to fall apart as the two-phase layer undergoes transition from bubbly to slug flow at higher inlet temperatures (i.e., lower subcoolings), especially at high heat fluxes. It should be noted that DHLM provided excellent predictions of pressure drop for all three smaller hydraulic diameters and its predictive accuracy increased at low heat fluxes. Relatively poor predictions for the largest hydraulic diameter may be related to strong entrance effects, especially at high Reynolds numbers, causing the assumption of constant mean liquid layer velocity in the model to be violated. Another reason for the deviation, which is mainly encountered at high fluxes, concerns both the aforementioned transition form bubbly to slug flow, and the flow instabilities (even flow reversal) at conditions approaching CHF as described in Ref. [27].

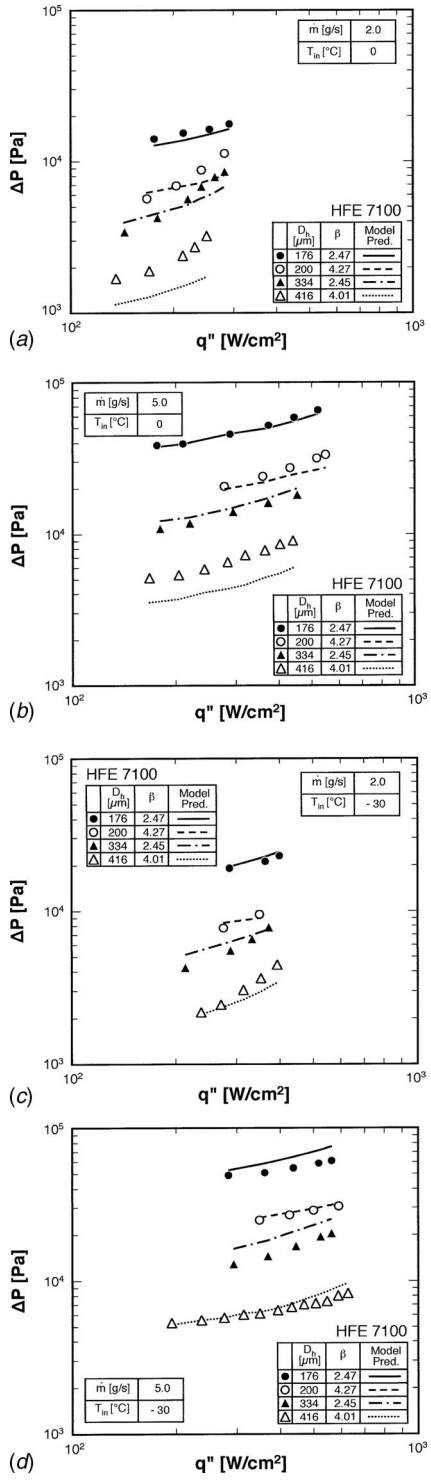

Fig. 8 Comparison of model predictions and measured variation in pressure drop with heat flux for (*a*) $T_{in}=0°C$ and $\dot{m}=2$ g/s, (*b*) $T_{in}=0°C$ and $\dot{m}=5$ g/s, (*c*) $T_{in}=-30°C$ and $\dot{m}=2$ g/s, and (*d*) $T_{in}=-30°C$ and $\dot{m}=5$ g/s

Figure 9 compares the model predictions with the entire pressure drop database of this study. Except for the large diameter data

Downloaded from https://asmedigitalcollection.asme.org/electronicpackaging/article-pdf/131/3/031008/5656138/031008_1.pdf by Purdue University at West Lafayette user on 22 October 2019

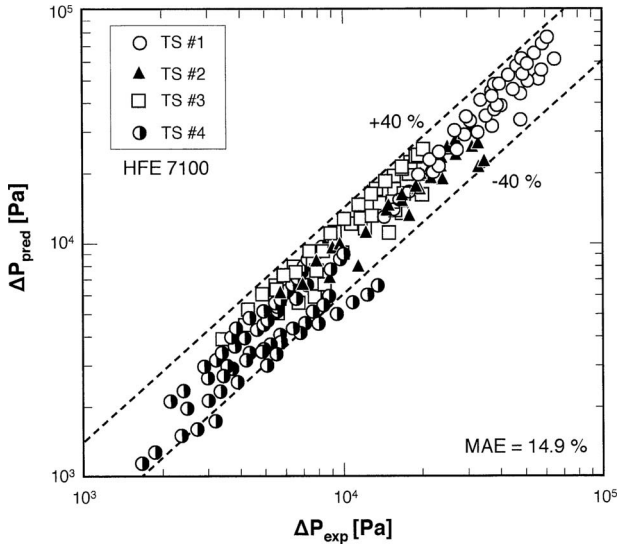

Fig. 9 Comparison of pressure drop predictions of DHLM and experimental data

corresponding to the higher inlet temperature, good predictions are achieved for most of the 191 data points, evidenced by a mean absolute error (MAE) of 14.9%.

5 Conclusions

This study examined subcooled boiling pressure drop in a microchannel heat sink. A new control volume model is proposed in which the subcooled flow is described as consisting of two layers: a homogeneous two-phase layer near the heated wall and a subcooled bulk liquid layer. Mass, momentum, and energy conservation equations are combined to predict pressure drop for thermodynamic equilibrium qualities below zero. Achieving closure in the construction of this developing homogeneous layer model required incorporating a relation for apparent quality across the two-phase layer as well as a new criterion for bubble departure. This model enables the determination of axial variations in two-phase layer thickness and velocity as well as pressure drop and is specifically tailored to rectangular microchannels. The model shows good predictions of pressure drop data for different mass velocities and subcoolings for four different microchannel sizes.

Acknowledgment

The authors are grateful for the support of the Office of Naval Research (ONR) for this research.

Nomenclature

A = cross-sectional area
C_G = dimensionless constant for rectangular microchannels
c_p = specific heat
D_h = hydraulic diameter of microchannel
f = friction factor
G = mass velocity
h = heat transfer coefficient; enthalpy
H_{ch} = height of microchannel
h_{fg} = latent heat of vaporization
K = friction constant for fully developed flow
K_i = interfacial mass flux
L = length of microchannel
$\dot{m}$ = mass flow rate of heat sink
N = number of microchannels in heat sink
P = pressure
ΔP = pressure drop
q'' = heat flux through heat sink base area
Re = Reynolds number
Re_{Dh} = Reynolds number based on microchannel hydraulic diameter
T = temperature
T^* = dimensionless temperature
TS = test section
U = mean layer velocity
W_{ch} = width of microchannel
W_w = width of solid wall separating microchannels
x' = apparent quality
Y^+ = dimensionless thickness of homogeneous two-phase layer
z = streamwise coordinate
Z^+ = dimensionless axial distance
z^+_{hy} = dimensionless length

Greek Symbols

β = aspect ratio
δ = thickness of homogeneous two-phase layer
μ = viscosity
ρ = density
τ = shear stress

Subscripts

bd = bubble departure from wall
ch = microchannel
exp = experimental
f = liquid layer; liquid
g = saturated vapor
H = homogeneous layer
i = interface between homogeneous two-phase layer and liquid layer
in = microchannel inlet
L = microchannel length
out = microchannel outlet
pred = predicted
sat = saturated
sub = subcooling
w = microchannel walls

References

[1] Mudawar, I., 2001, "Assessment of High-Heat-Flux Thermal Management Schemes," IEEE Trans. Compon. Packag. Technol., **24**, pp. 122–141.
[2] Lee, J., and Mudawar, I., 2005, "Two-Phase Flow in High-Heat-Flux Micro-Channel Heat Sink for Refrigeration Cooling Applications: Part I—Pressure Drop Characteristics," Int. J. Heat Mass Transfer, **48**, pp. 928–940.
[3] Lee, J., and Mudawar, I., 2005, "Two-Phase Flow in High-Heat-Flux Micro-Channel Heat Sink for Refrigeration Cooling Applications: Part II—Heat Transfer Characteristics," Int. J. Heat Mass Transfer, **48**, pp. 941–955.
[4] Lee, J., and Mudawar, I., 2006, "Implementation of Micro-Channel Evaporator for High-Heat-Flux Refrigeration Cooling Applications," ASME J. Electron. Packag., **128**, pp. 30–37.
[5] Kew, P. A., and Cornwell, K., 1997, "Correlations for the Prediction of Boiling Heat Transfer in Small-Diameter Channels," Appl. Therm. Eng., **17**, pp. 705–715.
[6] Ravigururajan, T. S., 1998, "Impact of Channel Geometry on Two-Phase Flow Heat Transfer Characteristics of Refrigerants in Microchannel Heat Exchangers," ASME J. Heat Transfer, **120**, pp. 485–491.
[7] Yan, Y.-Y., and Lin, T.-F., 1998, "Evaporation Heat Transfer and Pressure Drop of Refrigerant R-134a in a Small Pipe," Int. J. Heat Mass Transfer, **41**, pp. 4183–4194.
[8] Lee, H. J., and Lee, S. Y., 2001, "Heat Transfer Correlation for Boiling Flows in Small Rectangular Horizontal Channels With Low Aspect Ratios," Int. J. Multiphase Flow, **27**, pp. 2043–2062.
[9] Lin, S., Kew, P. A., and Cornwell, K., 2001, "Two-Phase Heat Transfer to a Refrigerant in a 1 mm Diameter Tube," Int. J. Refrig., **24**, pp. 51–56.
[10] Warrier, G. R., Dhir, V. K., and Momoda, L. A., 2002, "Heat Transfer and Pressure Drop in Narrow Rectangular Channels," Exp. Therm. Fluid Sci., **26**, pp. 53–64.
[11] Wen, D. S., Yan, Y., and Kenning, D. B. R., 2004, "Saturated Flow Boiling of Water in a Narrow Channel: Time-Averaged Heat Transfer Coefficient and Correlations," Appl. Therm. Eng., **24**, pp. 1207–1223.
[12] Huo, X., Chen, L., Tian, Y. S., and Karayiannis, T. G., 2004, "Flow Boiling and Flow Regimes in Small Diameter Tubes," Appl. Therm. Eng., **24**, pp. 1225–1239.

Downloaded from https://asmedigitalcollection.asme.org/electronicpackaging/article-pdf/131/3/031008/5656138/031008_1.pdf by Purdue University at West Lafayette user on 22 October 2019

[13] Lazarek, G. M., and Black, S. H., 1982, "Evaporative Heat Transfer, Pressure Drop and Critical Heat Flux in a Small Vertical Tube With R-113," Int. J. Heat Mass Transfer, **25**, pp. 945–959.
[14] Wambsganss, M. W., France, D. M., Jendrzejczyk, J. A., and Tran, T. N., 1993, "Boiling Heat Transfer in a Horizontal Small-Diameter Tube," ASME J. Heat Transfer, **115**, pp. 963–972.
[15] Tran, T. N., Wambsganss, M. W., and France, D. M., 1996, "Small Circular- and Rectangular-Channel Boiling With Two Refrigerants," Int. J. Multiphase Flow, **22**, pp. 485–498.
[16] Bao, Z. Y., Flectcher, D. F., and Haynes, B. S., 2000, "Flow Boiling Heat Transfer of Freon R11 and HCFC123 in Narrow Passages," Int. J. Heat Mass Transfer, **43**, pp. 3347–3358.
[17] Mehendale, S. S., and Jacobi, A. M., 2000, "Evaporative Heat Transfer in Mesoscale Heat Exchangers," ASHRAE Transactions: Symposia, Dallas, TX, pp. 445–452.
[18] Yu, W., France, D. M., Wambsganss, M. W., and Hull, J. R., 2002, "Two-Phase Pressure Drop, Boiling Heat Transfer, and Critical Heat Flux to Water in a Small-Diameter Horizontal Tube," Int. J. Multiphase Flow, **28**, pp. 927–941.
[19] Rouhani, S. Z., 1968, "Calculation of Steam Volume Fraction in Subcooled Boiling," ASME J. Heat Transfer, **90**, pp. 158–164.
[20] Levy, S., 1967, "Forced Convection Subcooled Boiling—Prediction of Vapor Volumetric Fraction," Int. J. Heat Mass Transfer, **10**, pp. 951–965.
[21] Saha, P., and Zuber, N., 1974, "Point of Net Vapor Generation and Vapor Void Fraction in Subcooled Boiling," *Proceedings of the 5th International Heat Transfer Conference*, Tokyo, Japan, Vol. 4, pp. 175–179.
[22] Kroeger, P. G., and Zuber, N., 1968, "An Analysis of the Effects of Various Parameters on the Average Void Fractions in Subcooled Boiling," Int. J. Heat Mass Transfer, **11**, pp. 211–213.
[23] Hoffman, M. A., and Wong, C. F., 1992, "Prediction of Pressure Drops in Forced Convection Subcooled Water Flows," Int. J. Heat Mass Transfer, **35**, pp. 3291–3299.
[24] Qu, W., and Mudawar, I., 2003, "Measurement and Prediction of Pressure Drop in Two-Phase Micro-Channel Heat Sinks," Int. J. Heat Mass Transfer, **46**, pp. 2737–2753.
[25] Qu, W., and Mudawar, I., 2003, "Flow Boiling Heat Transfer in Two-Phase Micro-Channel Heat Sinks—II. Annular Two-Phase Flow Model," Int. J. Heat Mass Transfer, **46**, pp. 2773–2784.
[26] Sturgis, J. C., and Mudawar, I., 1999, "Critical Heat Flux in a Long, Rectangular Channel Subjected to One-Sided Heating—II. Analysis of Critical Heat Flux Data," Int. J. Heat Mass Transfer, **42**, pp. 1849–1862.
[27] Lee, J., and Mudawar, I., 2008, "Fluid Flow and Heat Transfer Characteristics of Low Temperature Two-Phase Micro-Channel Heat Sinks—Part 1: Experimental Methods and Flow Visualization Results," Int. J. Heat Mass Transfer, **51**, pp. 4315–4326.
[28] Shah, R. K., and London, A. L., 1978, *Laminar Flow Forced Convection in Ducts: A Source Book for Compact Heat Exchanger Analytical Data*, Academic, New York, Supl. 1.
[29] Collier, J. G., and Thome, J. R., 1994, *Convective Boiling and Condensation*, 3rd ed., Oxford University, New York.

Downloaded from https://asmedigitalcollection.asme.org/electronicpackaging/article-pdf/131/3/031008/5656138/031008_1.pdf by Purdue University at West Lafayette user on 22 October 2019